

Geophysical Research Letters®

RESEARCH LETTER

10.1029/2021GL094638

Key Points:

- Global thermal-chemical subduction models with data-assimilation reproduced the evolution of East Asian stagnant slabs
- The key mechanism for slab stagnation is the westward mantle wind driven by continuous former Izanagi and Tethyan subduction
- Anisotropy calculations confirm the predominant upper-mantle depth of the mantle wind since the early Cenozoic

Supporting Information:

Supporting Information may be found in the online version of this article.

Correspondence to:

D. Peng and L. Liu,
dp6@illinois.edu;
ljiu@illinois.edu

Citation:

Peng, D., Liu, L., Hu, J., Li, S., & Liu, Y. (2021). Formation of East Asian stagnant slabs due to a pressure-driven Cenozoic mantle wind following Mesozoic subduction. *Geophysical Research Letters*, 48, e2021GL094638. <https://doi.org/10.1029/2021GL094638>

Received 14 JUN 2021

Accepted 26 AUG 2021

Formation of East Asian Stagnant Slabs Due To a Pressure-Driven Cenozoic Mantle Wind Following Mesozoic Subduction

Diandian Peng¹ , Lijun Liu¹ , Jiashun Hu², Sanzhong Li³ , and Yiming Liu^{1,4}

¹University of Illinois at Urbana-Champaign, Urbana, IL, USA, ²Southern University of Science and Technology, Shenzhen, China, ³Key Lab of Submarine Geoscience and Prospecting Techniques, MOE, Ocean University of China, Qingdao, China, ⁴China University of Petroleum (East China), Qingdao, China

Abstract The extensive fast seismic anomalies in the mantle transition zone beneath East Asia are often interpreted as stagnant Pacific slabs, and a reason for the widespread tectonics since the Mesozoic. Previous hypotheses for their formation mostly emphasize vertical resistances to slab penetration or trench retreat. In this study, we investigate the origin of these stagnant slabs using global-scale thermal-chemical models with data-assimilation. We find that subduction of the Izanagi-Pacific mid-ocean ridge marked the transition of mantle flow beneath western Pacific from being surface-driven Couette-type flow to pressure-driven Poiseuille-type flow, a result previously unrealized. This Cenozoic westward mantle wind driven by the pressure gradient independently explains seismic anisotropy in the region. We conclude that the mantle wind is the dominant mechanism for the formation of stagnant slabs by advecting them westward while the pressure gradient holds them in the transition zone.

Plain Language Summary The wide-spread flat lying fast seismic anomalies in the mantle transition zone are often referred to as stagnant slabs. The mechanisms for their formation are debated. In this study we use Earth-like global models to simulate slab geometry variation and reproduced the East Asian stagnant slabs. By running different tests we find that most previously proposed mechanisms are not the key reason, including the phase transformation at 660 km, viscosity increase in the lower mantle, seafloor age variation, and trench retreat. Instead, a westward mantle wind controlled the formation of stagnant slabs. This mantle wind occurred after the Izanagi-Pacific mid-ocean ridge began to subduct, and is driven by a long-lasting horizontal pressure gradient induced by previously subducted slabs. Without this mantle wind the slabs sink directly into the lower mantle. Seismic anisotropy models further confirm the dominant role of this upper-mantle flow in forming stagnant slabs.

1. Introduction

The term “stagnant slab” usually refers to the widely distributed fast seismic anomalies within the circum-Pacific mantle transition zones (MTZ) (Fukao et al., 2009; Huang & Zhao, 2006). There are several proposed mechanisms for why slabs can stagnate in the MTZ. The first one is related to the buoyancy associated with phase transformations of major mantle minerals, where both the negative Clapeyron slope of the ringwoodite-bridgmanite transformation (Christensen & Yuen, 1985; Tackley et al., 1993) and the delayed pyroxene-garnet transformation (King et al., 2015) tend to trap the slab within the MTZ. The second one is about the viscosity structure (Gurnis & Hager, 1988), where either a large viscosity increase into the lower mantle or a thin low-viscosity-layer right below the 660 km is invoked (Mao & Zhong, 2018). The third one concerns the age of the subducting plates, where a progressively older subducting slab tends to result in obvious trench retreat and stagnant slabs in the MTZ (Yang et al., 2018). The fourth one is the trench retreat, commonly attributed as an important reason for slab stagnation (Christensen, 1996; van der Hilst & Seno, 1993; Zhong & Gurnis, 1995). Some recent studies suggest the potential role of former subduction (Hu & Gurnis, 2020; Liu et al., 2021), but the dynamic nature remains elusive. There is still no systematic evaluation of these effects using a data-driven thermal-chemical modeling framework.

East Asia is an ideal location for studying subduction dynamics and slab stagnation. Numerous tomography models reveal high-velocity seismic anomalies in the MTZ beneath East Asia that are commonly interpreted as stagnant slabs (Huang & Zhao, 2006; Obayashi et al., 2013; van der Hilst et al., 1991). Regionally below

the North China Craton (NCC), the stagnant slab is found to be >1,500 km long east-west. Many surface tectonic events are suggested to be related to this abnormal subduction behavior (Ichiki et al., 2006). For example, the widespread intraplate volcanism since the Mesozoic (Richard et al., 2010; Zhao et al., 2009; Zheng et al., 2018) and the concurrent destruction of the NCC (Xu et al., 2009; Zhu et al., 2012) are often explained as a result of dehydration melting from the stagnant slabs that were assumed to be in existence since the Jurassic.

Despite the proposed significance of the East Asian stagnant slabs, the geological connections are mostly conceptual, and available geodynamic models supporting this idea are mostly two-dimensional (2D) in nature. There are some recent three-dimensional (3D) global models that reproduced the observed stagnant slabs (Ma et al., 2019; Mao & Zhong, 2018) but with different proposed mechanisms. This may reflect the fact that these studies used pure thermal models known to be incapable of emulating the dynamic evolution of upper-mantle slabs (Christensen, 1996; Hu et al., 2018). It is, therefore, important to study the 3D mantle evolution and far-field effects using more realistic thermal-chemical geodynamic models which can better simulate slab geometry and its evolution (Hu et al., 2018). In this study, we reproduced the spatial-temporal evolution of mantle flow and formation of stagnant slabs using global subduction models with a recent data-assimilation scheme (Supporting Information S1). The ~1.8 billion versatile chemical tracers capture the key buoyancy and viscosity features of the dynamic Earth, especially those at the lithospheric depths that previous models omitted. In particular, the resulting large lateral viscosity variation (4 orders of magnitude) across the subduction interface is critical for properly modeling the dynamic pressure and horizontal mantle flow (Coltice et al., 2019). We also consider a weak oceanic crust that can effectively decouple the plate interface upon subduction, a function that is similar to a sticky air layer (Crameri et al., 2012) for producing asymmetric subduction. To evaluate the debated mechanisms of slab stagnation, we consider the phase transformation and viscosity changes at 660 km depth, and performed models with different plate reconstructions, sea floor ages, and subduction histories. These data-driven models allow us to further explore previously unrealized mechanisms, such as our newly identified pressure-driven mantle wind that has been flowing westward around the Pacific and Philippine Sea slabs since the early Cenozoic.

2. Reproducing Present-Day Slabs

We first present the results from a reference model (Model 1), whose present-day slab structure is compared with seismic tomography. Model 1 runs from 200 Ma to the present day using the plate motion history and sea floor ages in a recent plate reconstruction (Figure S1) from Müller et al. (2016). At 500 km depth, there are wide-spread cold anomalies beneath East China (Figure 1a) whose spatial distribution is generally consistent with high-velocity P wave anomalies (Figures 1b and S2b) in GAP_P4 (Obayashi et al., 2013) and MIT_P08 (Li et al., 2008). The general consistency of the modeled cold anomalies with fast seismic anomalies beneath East Asia confirms the existence of stagnant slabs in the MTZ. Furthermore, we evaluate the model results from cross-sectional views. As seen in the temporal evolution of the Izanagi slab and Farallon slab (Figure S3), the slabs can evolve from high angle subduction to flat subduction, a key dynamic process not produced in the recent pure-thermal models (Ma et al., 2019; Mao & Zhong, 2018). For example, the well-recognized latest Cretaceous flat subduction of the Farallon slab (Coney & Reynolds, 1977; Liu et al., 2010; Saleeby, 2003) is predicted in our model (Figures S3i and S3j), but missing in previous studies.

In the lower mantle, the modeled slabs below East Asia are mainly large-scale features (Figures 1c and 1e) whose position and geometry are overall consistent with those of observed high-velocity seismic anomalies (Figures 1d, 1f, S2d, and S2f), with an improved match (Figures S3e, S3f, S3k, and S3l) than published models (Hu et al., 2018; Ma et al., 2019; Mao & Zhong, 2018). That the lower mantle slab is far from the trench supports the existence of a Cretaceous flat slab, as is the key for the new mechanism revealed in this work. In the upper mantle, our modeled stagnant slabs (Figures 1c and 1e) are also comparable to the high-velocity features (Figures 1d and 1f). At 32°N there are pieces of modeled stagnant slabs in the MTZ (Figure 1c), representing subducted Pacific and Philippine Sea Plates. These slab segments also correspond to tomography results with similarly segmented high-velocity anomalies above 660 km (Figures 1d and S2d). Along 43°N not only the stagnant Pacific slab is reproduced, the model also captures the increasing slab dip angle from the surface into the MTZ (Figure 1e), which is shown by tomography results (Figures 1f and S2f).

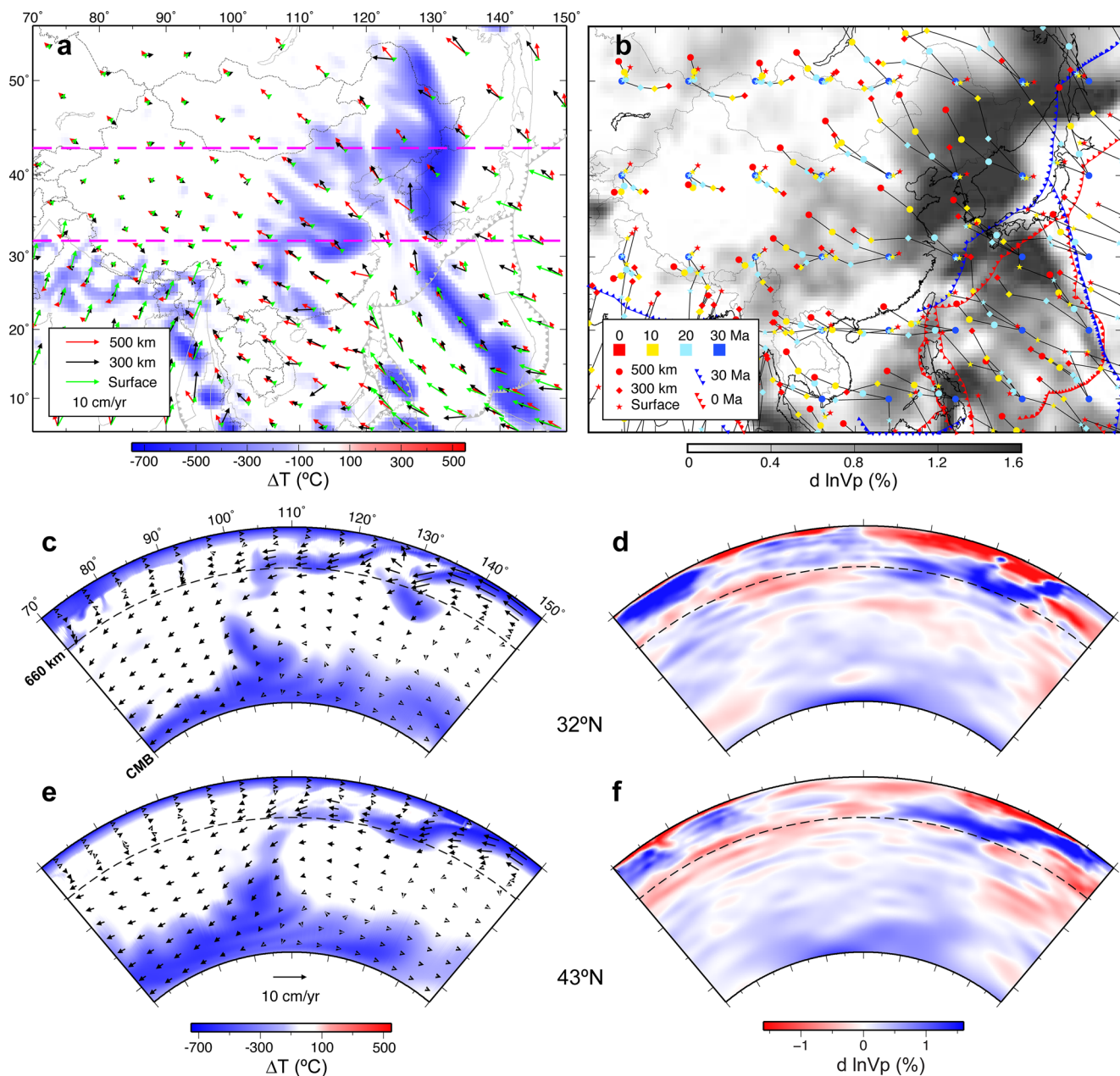


Figure 1. Comparison of Model 1 results and tomography. (a) Map view of modeled temperature at 500 km and velocities at 500 km, 300 km and on the surface. Magenta dashed lines mark the positions of two cross-sections along 32°N and 43°N. (b) Observed high-velocity P wave anomalies at 500 km in GAP_P4. Lateral migration of materials following the horizontal velocities (in the absence of vertical velocities) at 500 km (circles), 300 km (diamonds) and on the surface (stars) are shown with different colors representing different times. Trench locations at 30 Ma and the present day are also marked. (c) Present-day temperature and velocity along 32°N. (d) P wave anomalies in GAP_P4 along 32°N (e and f) same as (c and d) but along 43°N.

The variations in slab morphology mostly reflect the effect of the upper-mantle viscosity structure (Liu & Stegman, 2011).

To demonstrate that the formation of stagnant slabs is robust under different plate reconstructions, we present Model 2 whose surface kinematics are from Seton et al. (2012). Both the temporal evolution of slabs in this model (Figure S4) and the resulting present-day slab configuration are very similar to Model 1. In addition, the associated mantle flow and the formation of the stagnant slab remain largely unchanged too.

3. Evaluating Previous Mechanisms for Slab Stagnation

Next, we investigate the mechanism for the formation of these stagnant slabs. Earlier proposed mechanisms include phase transformations near 660 km (Christensen & Yuen, 1985; King et al., 2015; Tackley et al., 1993), viscosity increasing from the MTZ to the lower mantle (Gurnis & Hager, 1988), a low viscosity layer below 660 km (Mao & Zhong, 2018), age effects of the subducting plate (Yang et al., 2018), trench retreat (Christensen, 1996; van der Hilst & Seno, 1993; Zhong & Gurnis, 1995), or a combination of different mechanisms (Ma et al., 2019; Mao & Zhong, 2018; Yang et al., 2018). In Model 1, we include the Ringwoodite-Bridgmanite phase transformation at 660 km assuming a Clapron slope of -2 MPa/K (Marquardt & Miyagi, 2015) and a $30\times$ viscosity increase into the lower mantle (Figure S5). Both these factors tend to delay slabs from sinking into the lower mantle. However, they are apparently not enough to trap all slabs inside the MTZ, as can be clearly seen from the evolution of the Izanagi slab (Figures S3a and S3b) and the Farallon slab (Figures S3g and S3h). In both cases, the slab-tip becomes slightly flattened when passing through the 660-km discontinuity, showing the resistance encountered at this depth, but both slabs smoothly penetrated into the lower mantle with no significant delay. Thus, the global effects of phase transformation and viscosity increase near the 660 km depth cannot be a generic mechanism for stagnant slab formation.

To further test these viscosity effects, we perform three additional models (Models 3–5) that are similar to Model 1 but with modified viscosity structures (Figure S5b). Models 3 and 4 have a viscosity increase into the lower mantle by 10 and 100 times, respectively. Model 5 has a low viscosity layer below 660 km, as proposed in a recent global study (Mao & Zhong, 2018). Interestingly, all these models reproduce stagnant slabs (Figures 2b–2d) similar to those in Model 1 (Figure 2a). This means that slab stagnation is not very sensitive to the overall magnitude of lower mantle viscosity.

We also test the age effect of the subducting plate on slab evolution using the flexible data assimilation functions. The sea-floor age of the down-going Pacific plate has become progressively older toward the present day since the early Cenozoic (Figure S1), an observation recently proposed to cause slab stagnation beneath East Asia (Yang et al., 2018). To test this hypothesis, we design Model 6, which is identical to Model 1 except that the Pacific plate has a uniform age (50 Myr old) since 50 Ma. In this case, significant amounts of cold anomalies still accumulate in the MTZ forming stagnant structures (Figure 2e). Although the slab geometry has local differences relative to Model 1, the similar stagnant slabs suggest that the temporal change of the seafloor age is not the primary reason for the formation of these stagnant slabs.

Trench retreat has also been considered an important mechanism for the formation of stagnant slabs (Christensen, 1996; Goes et al., 2017; Ma et al., 2019; Mao & Zhong, 2018; van der Hilst & Seno, 1993; Zhong & Gurnis, 1995). Different from other hypotheses that focus on vertical forces, trench retreat emphasizes relative motion in the horizontal direction, thus representing an intuitive mechanism to explain the stagnant slabs. In a typical situation, the ocean-ward migration of the trench and the largely vertical sinking of the subducting plate cause a slab to lay flat in the MTZ (Christensen, 1996). Consequently, the horizontal length of the slab should be largely equivalent to the amount of trench retreat (Christensen, 1996). Recent plate reconstructions reveal that East Asia did experience trench retreat during the Cenozoic, but the amount of retreat is far less compared to the observed length of the stagnant slab. Beneath East Asia, the length of the stagnant part of the slab can exceed 1,500 km. As both our models and recent studies (Ma et al., 2019; Mao & Zhong, 2018) suggest, the stagnant slab is formed during the past 30 Ma. The corresponding amount of trench retreat is limited (Müller et al., 2016; Seton et al., 2012), as shown by the surface locations of the trenches over time (Figure 1b). Along 43°N, the maximum amount of trench retreat is about 7° during the past 30 Ma (Figure 1b), corresponding to a distance of $<600 \text{ km}$, which is far less than the length of stagnant slabs (Figures 1e and 1f). The same is true for the entire East Asia, where the amount of trench retreat is significantly less than the length of stagnant slabs (Fig. 1b). Thus, although trench retreat does contribute to the formation of stagnant slabs, it should not be the main mechanism.

4. A Cenozoic Mantle Wind Causing the Stagnant Slab

To better understand the dynamics of slab stagnation in our models, we analyze the mantle flow and the dynamic pressure which drives the flow. It has been shown (Hu et al., 2017) that the mantle below a subducting plate tends to experience a Couette-type flow driven by the surface plate motion (Figure S6a), and that

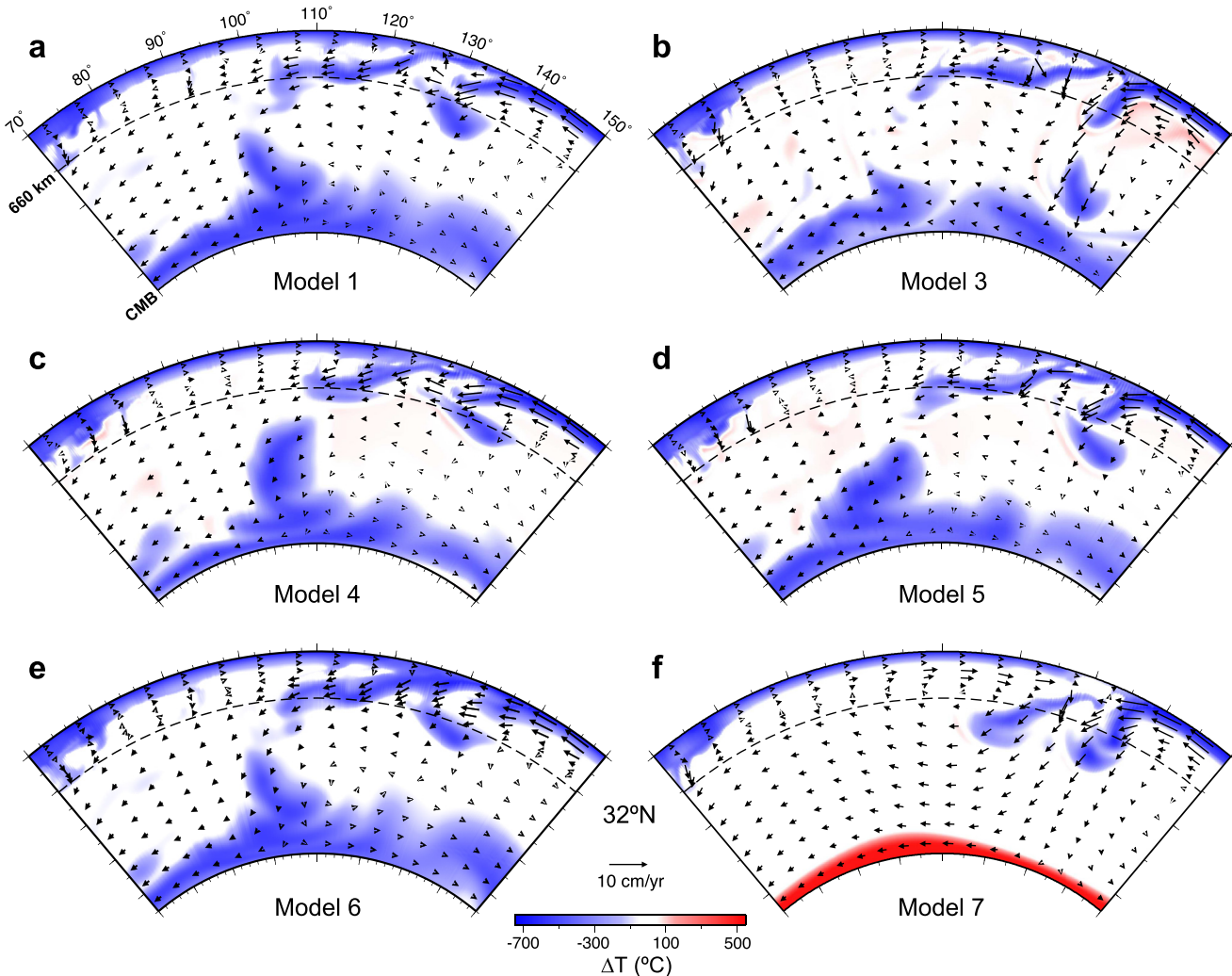


Figure 2. Vertical cross-sections of results in different models. (a–f) Present-day temperature and velocity along 32°N in models 1, 3–7, respectively. Note that model 3 and 4 has a viscosity increase into the lower mantle by 10 and 100 times, respectively. Model 5 has a low viscosity layer beneath 660 km. Model 6 has a 50-Myr-old seafloor after 50 Ma. Model 7 starts from 50 Ma with other parameters identical to Model 1.

below an overriding plate tends to display a trench-ward Poiseuille-type flow driven by the lateral pressure gradient (Figure S6b). According to our model results, continuous Cretaceous subduction of the Izanagi slab progressively reduced the dynamic pressure above the slab (Figures 3a–3c, Stevenson & Turner, 1977). By 100 Ma, the pressure gradient across the slab hinge was strong enough to reduce the dip angle of the Izanagi slab, which eventually became flat at 70 Ma (detailed discussion can be found in Peng & Liu, 2021). Such slab dip angle variation in response to the evolving gradient of the dynamic pressure is a natural result in our model, thus allowing us to study the dynamic evolution of the slabs. This represents a major improvement relative to studies with prescribed upper mantle slabs (e.g., Ma et al., 2019).

Before the arrival of the Izanagi-Pacific mid-ocean ridge (MOR) to the trench (Figures 3a–3c), the low pressure above the Izanagi slab excited a trench-ward Poiseuille-type flow beneath the overriding Asian plate (Figures 3b, 3c, and S7a). In contrast, beneath the subducting slab, the flow is of Couette-type, where the velocity magnitude decreases with depth, suggesting that the slab motion was driving the flow underneath. In this case, the Izanagi slab behaved as a mechanical barrier that separates the flow fields above it from those below. After the Izanagi-Pacific MOR entered the trench around 50 Ma (Müller et al., 2016), the Izanagi slab started to detach from the surface plate (Figures 3d and S7b). The gradual disappearance of the mechanical barrier (i.e., the strong slab) connected the low-pressure mantle above the Izanagi slab directly

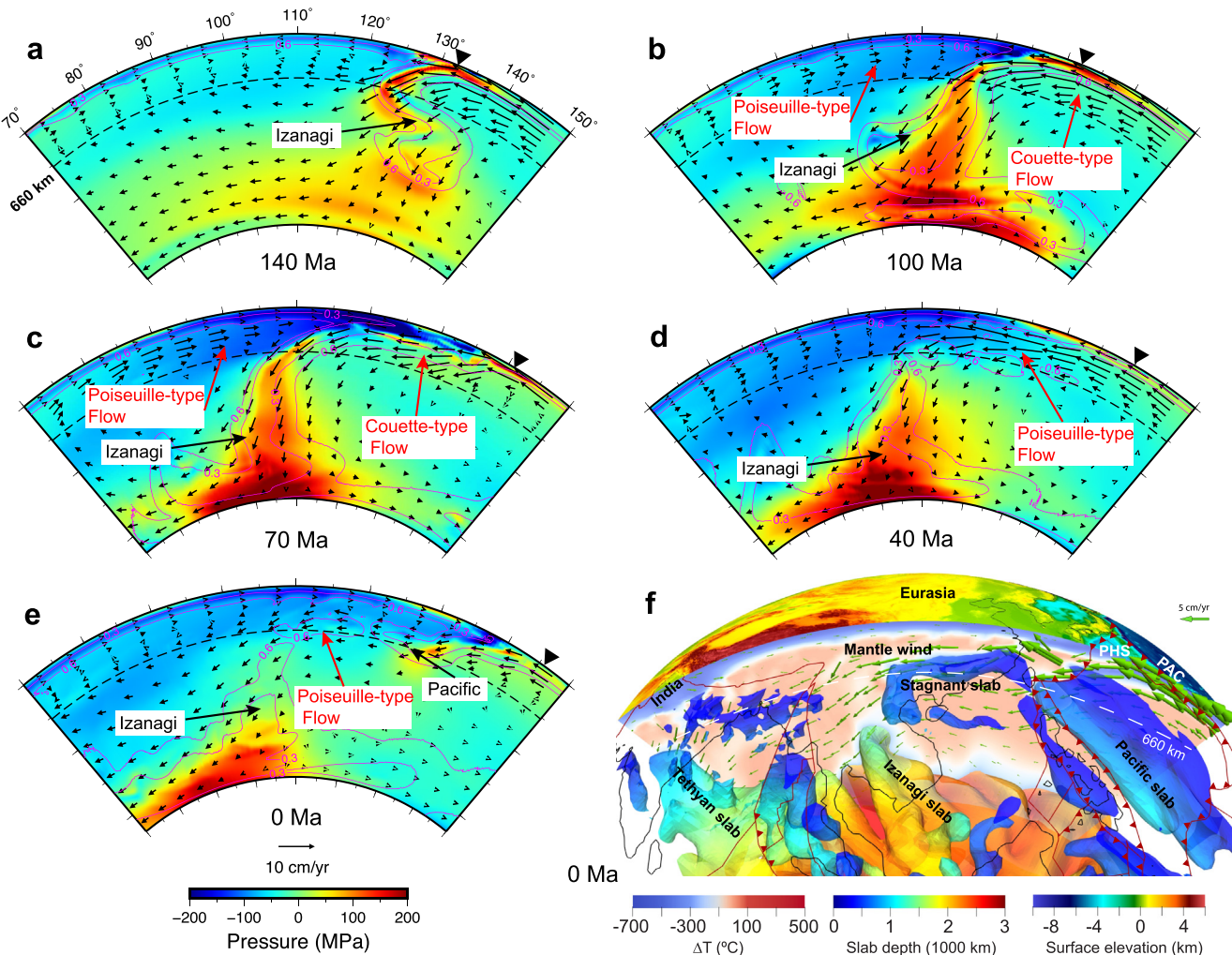


Figure 3. Evolution of the dynamic pressure and mantle flow in Model 1 (a–e) Dynamic pressure and velocity along 43°N at 140 Ma, 100 Ma, 70 Ma, 40 Ma, and the present day. Magenta contours show non-dimensional geotherms at 0.3 (-400°C) and 0.6 (-100°C). Black triangles show the trench positions. Annotations indicate different flow patterns and show a switch of mantle flow patterns below East Asia from being Couette-type in the latest Cretaceous to Poiseuille-type in the Cenozoic. (f) 3D view of the present-day slabs and velocity and observed topography. Slabs colored by depth are represented as isovolumes with non-dimensional temperature lower than 0.45 (-250°C). The vertical cross-section shows temperature.

with the high-pressure asthenosphere beneath the sinking MOR (Figures 3d and S7b). Consequently, the flow beneath the incoming Pacific Plate became dramatically different from before. This is because the newly established sharp lateral pressure-gradient across the MOR excited a fast westward Poiseuille-type flow from below the incoming Pacific Plate to above the sinking Izanagi slab (Figure 3d). This westward Poiseuille-type flow originating from beneath both the subducting Pacific Plate and Philippine Sea Plate covered most of East Asia (Figure 1a) and was maintained throughout the Cenozoic (Figures 3d–3f, S7b, and S7c). During this course, sinking of the Izanagi slab extended the low-pressure mantle wedge downward, causing the westward flow to expand from initially within the upper mantle (Figure 3d) to the MTZ and uppermost lower mantle at the present (Figure 3e).

A close examination reveals that the Tethyan subduction on the west since the Mesozoic (Figure 3) also contributes to the broad low dynamic pressure region beneath the Asian continent, forming an asymmetric, whole-mantle scale flow pattern beneath East Asia with a net westward velocity throughout the entire mantle depth. This evolving dynamic pressure and mantle flow occurred beneath most of East Asia, largely following the trajectory of the sinking Izanagi slab (Figures 1 and 3). In a map view, the mantle velocities at 500 and 300 km below the entire East Asian continent are notably larger in amplitude than those at the

surface (Figure 1a). Effectively, this strong Poiseuille-type flow acted as a regional mantle wind that carried the subducting Pacific and Philippine Sea slabs toward the west while the pressure gradient across the slabs was lifting them and thus preventing them from entering the lower mantle. Calculations show that the East Asian upper mantle flowed westward for a distance well over 1,000 km since 30 Ma, comparable to the length of the observed stagnant slab (Figure 1b). Carried by this mantle wind, the slab can travel westward easily to form a >1,500-km-long stagnant slab. This mantle wind has also been consistently generated in other models using different plate reconstructions and viscosity structures (Models 2–5; Figures 2b–2d and S4). These results suggest that this mantle wind is a robust feature which acts as the key mechanism for the observed slab stagnation.

In order to further verify that the westward mantle wind is necessary for the formation of stagnant slabs, we run Model 7 which starts only from 50 Ma but with other parameters identical to Model 1. Since no prior subduction is included, there are no former slabs to induce the Poiseuille-type flow beneath East Asia. Consequently, the lack of a regional mantle wind causes the Pacific and Philippine Sea slabs to subduct more steeply (Figure S8) than that in Model 1 (Figures 1c and 1e). Eventually, both slabs penetrated the 660 km discontinuity at the present day (Figures 2f and S8). Since Model 7 has the same phase transformations, viscosity structure, sea floor age, and amount of Cenozoic trench retreat as in Model 1, and the contrasting fates of the western Pacific slabs in these two models confirm that the westward mantle wind, driven by former slabs, is key for the slab stagnation.

An important validation for the existence and effects of the above identified mantle wind comes from seismic anisotropy. Since seismic anisotropy reflects the cumulative deformation of the mantle during the geological past (Faccenda & Capitanio, 2013; Hu et al., 2017), we calculate the present-day anisotropy based on mantle flow since 40 Ma in Model 1 (Supporting Information S1). The comparison between the predicted flow-induced lattice preferred orientation (LPO) and observed surface wave anisotropy (Yuan & Beghein, 2013) at the asthenosphere depth reveals a remarkably good match of directions with an average misfit of 23.6° beneath most of East Asia (Figure 4a). The dominantly east-west fast anisotropy directions in East Asia (Figure 4a) are due to the westward mantle wind (Figure 1a).

In addition, land-based shear wave splitting (SWS) measurements provide an independent constraint on the depth-integrated rock fabrics due to mantle deformation (Hu et al., 2017; Long & Becker, 2010). Due to the small lithosphere thickness in East Asia (Zhang et al., 2019), the lithospheric contribution to SWS is likely minor. Therefore, we use this region to further examine our geodynamic model with SWS data (Supporting Information S1). Remarkably, the predicted SWS in East Asia matches the observed SWS anisotropy in the fast directions throughout the region, with a 23.9° angular misfit (Figures 4b and S9). This region is also where the prominent mantle wind occurs at depth (Figure 1a). It is important to note that the pattern of SWS (Figure 4b) closely follows that of surface wave anisotropy (Figure 4a) across East Asia, an observation further verifying the similar direction of the westward mantle wind through upper-mantle depth (Figures 1a, 3d and 3e). Consequently, these seismic anisotropy analyses strongly support the role of the westward mantle wind in shaping the observed stagnant slabs.

5. Conclusion and Implications

Collectively, our results show that the enduring dynamic pressure gradient, as a result of former subduction, drives the slab dip angle variation since the Mesozoic. The Cenozoic mantle wind beneath East Asia induced by this pressure gradient during the transition from Mesozoic Izanagi and Tethyan to Cenozoic Pacific subduction is critical for the formation of the stagnant slab beneath East Asia. During this process, the Izanagi-Pacific MOR subduction is a turning point for the change of the flow pattern beneath the slabs subducting below the east coast of Asia. Although the exact timing of the MOR subduction is debated (Arculus et al., 2015; Li et al., 2012; Miyazaki et al., 2015; Seton et al., 2015), these works agree that it happened 60–50 Ma. This uncertainty will not affect our conclusion about the formation of the westward mantle wind and slab stagnation. The finding that the Mesozoic Izanagi slab still controls the Cenozoic subduction and mantle evolution echoes the recent findings that the former Farallon slab now mostly under the east coast of North America still plays an important role in mantle processes below the western United States (Zhou,

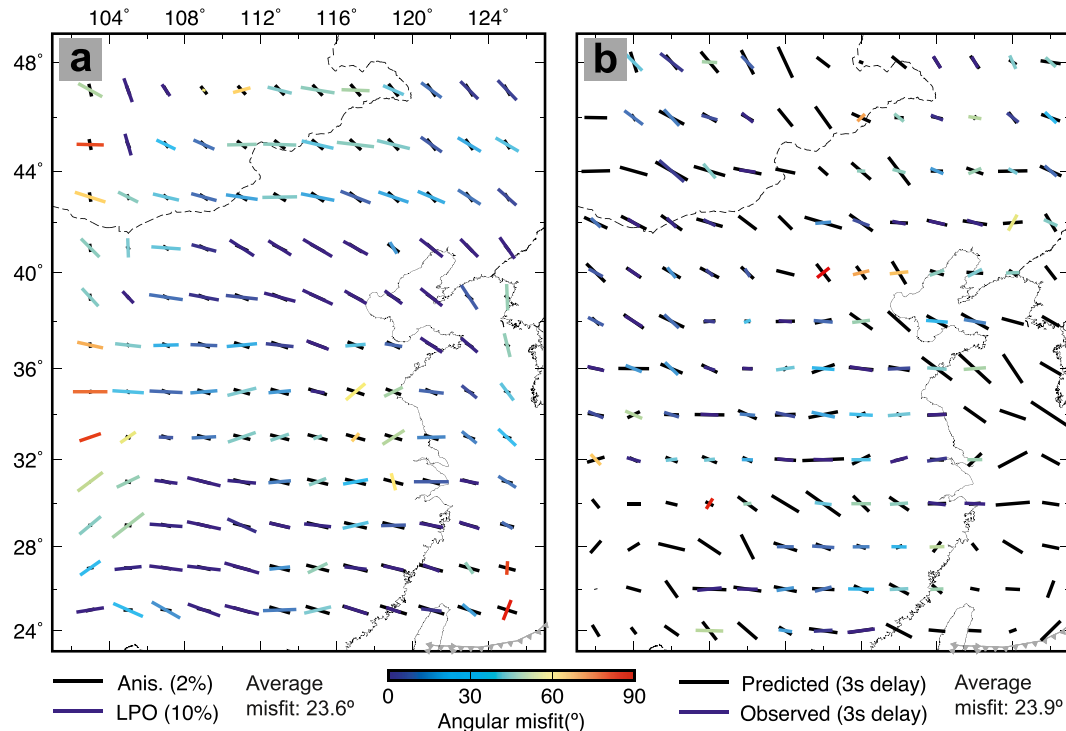


Figure 4. Predicted and observed seismic anisotropy. The prediction is based on the mantle flow in Model 1. (a) Comparison of the observed (Yuan & Beghein, 2013) and predicted azimuthal anisotropy beneath East Asia at an asthenosphere depth (230 km). Black bars show observed anisotropy. Color bars show predicted anisotropy represented by the orientation of the TI axis (symmetry axis of the transverse isotropy) of the lattice preferred orientation (LPO). Model results are projected to the observation points, with color showing angular misfit with data. (b) Comparison between observed and predicted SWS anisotropy. Black bars show predicted shear wave splitting (SWS). Color bars show regionally smoothed SWS data (see Figure S9 for the full data collection) and angular misfit with prediction.

Hu, et al., 2018; Zhou, Liu, et al., 2018). Consequently, this reveals the long-lasting dynamic effect of ancient subduction.

This study also generates several other new insights on mantle dynamics and regional tectonics. First, many previous hypotheses for stagnant slab formation emphasize the vertical resistance (such as the viscosity jump at 660 km) for slab penetration into the lower mantle. By showing that the East Asian stagnant slab represents a combined result of ridge subduction and long-lasting Mesozoic subduction, we reveal that vertical mantle resistance plays a limited role in prohibiting slab penetration into the lower mantle, and also explains why slabs at other times and locations can smoothly sink into the lower mantle. Second, it is still unclear why and how the Izanagi-Pacific MOR and adjacent young seafloors can subduct during the early Cenozoic, given their apparent buoyancy that resists subduction. The presence of the Poiseuille-type flow below the western Pacific could have actively entrained the buoyant MOR into the subduction zone during early Cenozoic (Figure 3). Therefore, the landward mantle wind may act as a generic driving force of ridge subduction (Sun et al., 2018). Finally, the model results showing that the East Asian stagnant slab formed only during the late-Cenozoic suggest no direct connection between this slab and the Mesozoic tectonics of East Asia as speculated in previous studies (Zheng et al., 2018; Zhu et al., 2012).

Data Availability Statement

The original version of CitcomS is available at www.geodynamics.org/cig/software/citcoms/. GPlates can be accessed at www.gplates.org/. Tools used to make the figures are available at <https://www.generic-mapping-tools.org/> and www.paraview.org/. The anisotropy code DRex is available at <http://www.ipgp.fr/~kaminski/> and FSTRACK is available at <http://www-udc.ig.utexas.edu/external/becker/data.html>. The P-wave tomography model GAP_P4 is available at http://d-earth.jamstec.go.jp/GAP_P4/. The P-wave

tomography model MIT_P08 is within the paper and its Supporting Information S1. The surface wave anisotropy models YB13SVani (Yuan & Beghein, 2013) are available at <https://faculty.epss.ucla.edu/~cbeghein/research/global-tomography/sv-anisotropy-mantle-transition-zone>. SWS splitting data (Chang et al., 2017; Chen et al., 2017; Li et al., 2018; Qiang et al., 2017; Shi et al., 2015; Yang et al., 2019; Yu & Chen, 2016) can be accessed at <https://ds.iris.edu/spud/swsmeasurement/>. The data for numerical results of Model 1 and related plotting scripts are available at Zenodo (<https://doi.org/10.5281/zenodo.3884294>).

Acknowledgments

The authors sincerely thank Bernhard Steinberger, an anonymous reviewer, and editor Lucy Flesch for their constructive suggestions on the manuscript. This study is supported by NSF funding EAR1554554.

References

- Arculus, R. J., Ishizuka, O., Bogus, K. A., Gurnis, M., Hickey-Vargas, R., Aljahdali, M. H., et al. (2015). A record of spontaneous subduction initiation in the Izu-Bonin-Mariana arc. *Nature Geoscience*, 8(9), 728–733. <https://doi.org/10.1038/ngeo2515>
- Chang, L., Ding, Z., Wang, C., & Flesch, L. M. (2017). Vertical coherence of deformation in lithosphere in the NE margin of the Tibetan plateau using GPS and shear-wave splitting data. *Tectonophysics*, 699, 93–101. <https://doi.org/10.1016/j.tecto.2017.01.025>
- Chen, H., Niu, F., Obayashi, M., Grand, S. P., Kawakatsu, H., John Chen, Y., et al. (2017). Mantle seismic anisotropy beneath NE China and implications for the lithospheric delamination hypothesis beneath the southern Great Xing'an range. *Earth and Planetary Science Letters*, 471, 32–41. <https://doi.org/10.1016/j.epsl.2017.04.030>
- Christensen, U. R. (1996). The influence of trench migration on slab penetration into the lower mantle. *Earth and Planetary Science Letters*, 140(1–4), 27–39. [https://doi.org/10.1016/0012-821X\(96\)00023-4](https://doi.org/10.1016/0012-821X(96)00023-4)
- Christensen, U. R., & Yuen, D. A. (1985). Layered convection induced by phase transitions. *Journal of Geophysical Research*, 90(B12), 10291. <https://doi.org/10.1029/jb090ib12p10291>
- Coltice, N., Husson, L., Faccenna, C., & Arnould, M. (2019). What drives tectonic plates? *Science Advances*, 5(10), eaax4295. <https://doi.org/10.1126/sciadv.aax4295>
- Coney, P. J., & Reynolds, S. J. (1977). Cordilleran Benioff zones. *Nature*, 270(5636), 403–406. <https://doi.org/10.1038/270403a0>
- Crameri, F., Tackley, P. J., Meilick, I., Gerya, T. V. & Kaus, B. J. A. (2012). A free plate surface and weak oceanic crust produce single-sided subduction on Earth. *Geophysical Research Letters*, 39(3). <https://doi.org/10.1029/2011GL050046>
- Faccenda, M., & Capitanio, F. A. (2013). Seismic anisotropy around subduction zones: Insights from three-dimensional modeling of upper mantle deformation and SKS splitting calculations. *Geochemistry, Geophysics, Geosystems*, 14(1), 243–262. <https://doi.org/10.1002/ggge.20055>
- Fukao, Y., Obayashi, M., & Nakakuki, T. (2009). Stagnant slab: A review. *Annual Review of Earth and Planetary Sciences*, 37(1), 19–46. <https://doi.org/10.1146/annurev.earth.36.031207.124224>
- Goes, S., Agrusta, R., van Hunen, J., & Garel, F. (2017). Subduction-transition zone interaction: A review. *Geosphere*, 13(3), 644–664. <https://doi.org/10.1130/GES01476.1>
- Gurnis, M., & Hager, B. H. (1988). Controls of the structure of subducted slabs. *Nature*, 335, 317–321. <https://doi.org/10.1038/335317a0>
- Hu, J., Faccenda, M., & Liu, L. (2017). Subduction-controlled mantle flow and seismic anisotropy in South America. *Earth and Planetary Science Letters*, 470, 13–24. <https://doi.org/10.1016/j.epsl.2017.04.027>
- Hu, J., & Gurnis, M. (2020). Subduction duration and lab dip. *Geochemistry, Geophysics, Geosystems*, 21(4), 1–24. <https://doi.org/10.1029/2019GC008862>
- Hu, J., Liu, L., Zhou, Q., & Zhou, Q. (2018). Reproducing past subduction and mantle flow using high-resolution global convection models. *Earth and Planetary Physics*, 2(3), 189–207. <https://doi.org/10.26464/ep2018019>
- Huang, J., & Zhao, D. (2006). High-resolution mantle tomography of China and surrounding regions. *Journal of Geophysical Research*, 111(9), 1–21. <https://doi.org/10.1029/2005JB004066>
- Ichiki, M., Baba, K., Obayashi, M., & Utada, H. (2006). Water content and geotherm in the upper mantle above the stagnant slab: Interpretation of electrical conductivity and seismic P-wave velocity models. *Physics of the Earth and Planetary Interiors*, 155(1–2), 1–15. <https://doi.org/10.1016/j.pepi.2005.09.010>
- King, S. D., Frost, D. J., & Rubie, D. C. (2015). Why cold slabs stagnate in the transition zone. *Geology*, 43(3), 231–234. <https://doi.org/10.1130/G36320.1>
- Li, C., Van Der Hilst, R. D., Engdahl, E. R., & Burdick, S. (2008). A new global model for P wave speed variations in Earth's mantle. *Geochemistry, Geophysics, Geosystems*, 9(5), a–n. <https://doi.org/10.1029/2007GC001806>
- Li, H., Ling, M. X., Li, C. Y., Zhang, H., Ding, X., Yang, X. Y., et al. (2012). A-type granite belts of two chemical subgroups in central eastern China: Indication of ridge subduction. *Lithos*, 150, 26–36. <https://doi.org/10.1016/j.lithos.2011.09.021>
- Li, H., Song, X., Lü, Q., Yang, X., Deng, Y., Ouyang, L., et al. (2018). Seismic imaging of lithosphere structure and upper mantle deformation beneath east-central China and their tectonic implications. *Journal of Geophysical Research: Solid Earth*, 123(4), 2856–2870. <https://doi.org/10.1002/2017JB014992>
- Liu, L., Gurnis, M., Seton, M., Saleeby, J., Müller, R. D., & Jackson, J. M. (2010). The role of oceanic plateau subduction in the Laramide orogeny. *Nature Geoscience*, 3(5), 353–357. <https://doi.org/10.1038/ngeo829>
- Liu, L., & Stegman, D. R. (2011). Segmentation of the Farallon slab. *Earth and Planetary Science Letters*, 311(1–2), 1–10. <https://doi.org/10.1016/j.epsl.2011.09.027>
- Liu, S., Ma, P., Zhang, B., & Gurnis, M. (2021). The horizontal slab beneath East Asia and its subdued surface dynamic response. *Journal of Geophysical Research: Solid Earth*, 126(3). <https://doi.org/10.1029/2020JB021156>
- Long, M. D., & Becker, T. W. (2010). Mantle dynamics and seismic anisotropy. *Earth and Planetary Science Letters*, 297(3–4), 341–354. <https://doi.org/10.1016/j.epsl.2010.06.036>
- Ma, P., Liu, S., Gurnis, M., & Zhang, B. (2019). Slab horizontal subduction and slab tearing beneath East Asia. *Geophysical Research Letters*, 46(10), 5161–5169. <https://doi.org/10.1029/2018GL081703>
- Mao, W., & Zhong, S. (2018). Slab stagnation due to a reduced viscosity layer beneath the mantle transition zone. *Nature Geoscience*, 11(11), 876–881. <https://doi.org/10.1038/s41561-018-0225-2>
- Marquardt, H., & Miyagi, L. (2015). Slab stagnation in the shallow lower mantle linked to an increase in mantle viscosity. *Nature Geoscience*, 8(4), 311–314. <https://doi.org/10.1038/ngeo2393>

- Miyazaki, T., Kimura, J.-I., Senda, R., Vaglarov, B. S., Chang, Q., Takahashi, T., et al. (2015). Missing western half of the Pacific Plate: Geochemical nature of the Izanagi-Pacific Ridge interaction with a stationary boundary between the Indian and Pacific mantles. *Geochemistry, Geophysics, Geosystems*, 16(9), 3309–3332. <https://doi.org/10.1002/2015GC005911>
- Müller, R. D., Seton, M., Zahirovic, S., Williams, S. E., Matthews, K. J., Wright, N. M., et al. (2016). Ocean basin evolution and global-scale plate reorganization events since pangea breakup. *Annual Review of Earth and Planetary Sciences*, 44(1), 107–138. <https://doi.org/10.1146/annurev-earth-060115-012211>
- Obayashi, M., Yoshimitsu, J., Nolet, G., Fukao, Y., Shiobara, H., Sugioka, H., et al. (2013). Finite frequency whole mantle P wave tomography: Improvement of subducted slab images. *Geophysical Research Letters*, 40(21), 5652–5657. <https://doi.org/10.1029/2013GL057401>
- Peng, D., & Liu, L. (2021). A newly discovered Late-Cretaceous East Asian flat slab explains its unique lithospheric structure and tectonics. *Earth and Space Science Open Archive*. <https://doi.org/10.1002/essoar.10506583.1>
- Qiang, Z., Wu, Q., Li, Y., Gao, M., Demberel, S., Ulzibat, M., et al. (2017). Complicated seismic anisotropy beneath south-central Mongolia and its geodynamic implications. *Earth and Planetary Science Letters*, 465, 126–133. <https://doi.org/10.1016/j.epsl.2017.02.035>
- Richard, G. C., Iwamori, H., Suetsugu, D., Bina, C., Inoue, T., Wiens, D., & Jellinek, M. (2010). Stagnant slab, wet plumes and Cenozoic volcanism in East Asia. *Physics of the Earth and Planetary Interiors*, 183(1–2), 280–287. <https://doi.org/10.1016/j.pepi.2010.02.009>
- Saleeby, J. (2003). Segmentation of the Laramide Slab - Evidence from the southern Sierra Nevada region. *Bulletin of the Geological Society of America*, 115(6), 655–668. [https://doi.org/10.1130/0016-7606\(2003\)115<0655:SOTLSF>2.0.CO;2](https://doi.org/10.1130/0016-7606(2003)115<0655:SOTLSF>2.0.CO;2)
- Seton, M., Flament, N., Whittaker, J., Müller, R. D., Gurnis, M., & Bower, D. J. (2015). Ridge subduction sparked reorganization of the Pacific plate-mantle system 60–50 million years ago. *Geophysical Research Letters*, 42(6), 1732–1740. <https://doi.org/10.1002/2015GL063057>
- Seton, M., Müller, R. D., Zahirovic, S., Gaina, C., Torsvik, T., Shephard, G., et al. (2012). Global continental and ocean basin reconstructions since 200Ma. *Earth-Science Reviews*, 113(3–4), 212–270. <https://doi.org/10.1016/j.earscirev.2012.03.002>
- Shi, Y., Gao, Y., Tai, L., & Fu, Y. (2015). The shear-wave splitting in the crust and the upper mantle around the Bohai Sea, North China. *Journal of Asian Earth Sciences*, 111, 505–516. <https://doi.org/10.1016/j.jseas.2015.06.015>
- Stevenson, D. J., & Turner, J. S. (1977). Angle of subduction. *Nature*, 270(5635), 334–336. <https://doi.org/10.1038/270334a0>
- Sun, W., Liu, L., Hu, Y., Ding, W., Liu, J., Ling, M., et al. (2018). Post-ridge-subduction acceleration of the Indian plate induced by slab rollback. *Solid Earth Sciences*, 3(1), 1–7. <https://doi.org/10.1016/j.sesci.2017.12.003>
- Tackley, P. J., Stevenson, D. J., Glatzmaier, G. A., & Schubert, G. (1993). Effects of an endothermic phase transition at 670 km depth on spherical mantle convection. *Nature*, 361, 699–704. <https://doi.org/10.1038/361699a0>
- vander Hilst, R., Engdahl, R., Spakman, W., & Nolet, G. (1991). Tomographic imaging of subducted lithosphere below northwest Pacific island arcs. *Nature*, 353(6339), 37–43. <https://doi.org/10.1038/353037a0>
- vander Hilst, R., & Seno, T. (1993). Effects of relative plate motion on the deep structure and penetration depth of slabs below the Izu-Bonin and Mariana island arcs. *Earth and Planetary Science Letters*, 120(3–4), 395–407. [https://doi.org/10.1016/0012-821X\(93\)90253-6](https://doi.org/10.1016/0012-821X(93)90253-6)
- Xu, Y. G., Li, H. Y., Pang, C. J., & He, B. (2009). On the timing and duration of the destruction of the North China Craton. *Chinese Science Bulletin*, 54(19), 3379–3396. <https://doi.org/10.1007/s11434-009-0346-5>
- Yang, T., Moresi, L., Zhao, D., Sandiford, D., & Whittaker, J. (2018). Cenozoic lithospheric deformation in Northeast Asia and the rapidly-aging Pacific Plate. *Earth and Planetary Science Letters*, 492, 1–11. <https://doi.org/10.1016/j.epsl.2018.03.057>
- Yang, X., Li, H., Li, Y., Lü, Q., Zhang, G., Jiang, G., & Li, X. (2019). Seismic anisotropy beneath eastern China from shear wave splitting. *Geophysical Journal International*, 218(3), 1642–1651. <https://doi.org/10.1093/gji/gjz242>
- Yu, Y., & Chen, Y. J. (2016). Seismic anisotropy beneath the southern Ordos block and the Qinling-Dabie orogen, China: Eastward Tibetan asthenospheric flow around the southern Ordos. *Earth and Planetary Science Letters*, 455, 1–6. <https://doi.org/10.1016/j.epsl.2016.08.026>
- Yuan, K., & Beghein, C. (2013). Seismic anisotropy changes across upper mantle phase transitions. *Earth and Planetary Science Letters*, 374, 132–144. <https://doi.org/10.1016/j.epsl.2013.05.031>
- Zhang, Y., Chen, L., Ai, Y., & Jiang, M. (2019). Lithospheric structure beneath the central and western North China Craton and adjacent regions from S-receiver function imaging. *Geophysical Journal International*, 219(1), 619–632. <https://doi.org/10.1093/gji/gjz322>
- Zhao, D., Tian, Y., Lei, J., Liu, L., & Zheng, S. (2009). Seismic image and origin of the Changbai intraplate volcano in East Asia: Role of big mantle wedge above the stagnant Pacific slab. *Physics of the Earth and Planetary Interiors*, 173(3–4), 197–206. <https://doi.org/10.1016/j.pepi.2008.11.009>
- Zheng, Y., Xu, Z., Zhao, Z., & Dai, L. (2018). Mesozoic mafic magmatism in North China: Implications for thinning and destruction of cratonic lithosphere. *Science China Earth Sciences*, 61, 353–385. <https://doi.org/10.1007/s11430-017-9160-3>
- Zhong, S., & Gurnis, M. (1995). Mantle convection with plates and mobile, faulted plate margins. *Science*, 267(5199), 838–843. <https://doi.org/10.1126/science.267.5199.838>
- Zhou, Q., Hu, J., Liu, L., Chaparro, T., Stegman, D. R., & Faccenda, M. (2018). Western U.S. seismic anisotropy revealing complex mantle dynamics. *Earth and Planetary Science Letters*, 500, 156–167. <https://doi.org/10.1016/j.epsl.2018.08.015>
- Zhou, Q., Liu, L., & Hu, J. (2018). Western US volcanism due to intruding oceanic mantle driven by ancient Farallon slabs. *Nature Geoscience*, 11(1), 70–76. <https://doi.org/10.1038/s41561-017-0035-y>
- Zhu, R. X., Xu, Y. G., Zhu, G., Zhang, H. F., Xia, Q. K., & Zheng, T. Y. (2012). Destruction of the North China Craton. *Science China Earth Sciences*, 55(10), 1565–1587. <https://doi.org/10.1007/s11430-012-4516-y>